Atmospheric mesoscale modeling to simulate annual and seasonal wind speeds for wind energy production in Mexico

Sustainable Energy Technologies and Assessments 68 (2024) 103848

Contents lists available at ScienceDirect

Sustainable Energy Technologies and Assessments

journal homepage: www.elsevier.com/locate/seta

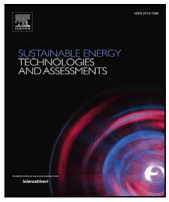

Atmospheric mesoscale modeling to simulate annual and seasonal wind speeds for wind energy production in Mexico

J.G. Hernandez-Yepes [a,*], O. Rodriguez-Hernandez [b], C.A. Lopez-Villalobos [b], O. Martínez-Alvarado [c]

[a] Posgrado en Ingeniería, Universidad Nacional Autónoma de Mexico, Priv. Xochicalco S/N, Temixco, 62580, Morelos, Mexico
[b] Instituto de Energías Renovables, Universidad Nacional Autónoma de Mexico, Priv. Xochicalco S/N, Temixco, 62580, Morelos, Mexico
[c] Department of Meteorology, National Centre for Atmospheric Science, University of Reading, Harry Pitt Building, Whiteknights Road, Earley Gate, Reading, RG6 6ES, United Kingdom

ARTICLE INFO

Dataset link: https://github.com/heyej/Mexico-WRF-wind-speed

Keywords:
Annual and seasonal capacity factor estimation
Wind energy variability
Regional mesoscale atmospheric modeling
Wind speed and capacity factor forecasting
High resolution numerical simulation

ABSTRACT

Numerical models have been used widely to reproduce wind resources around the globe. Mexico's vast territory has a wide range of geographical characteristics with abundant wind potential. This work explores WRF simulations applied to reproduce the wind speed and capacity factor (CF) of 22 wind masts, organized into seven regions delimited by geographic conditions and consisting of 33 years of data. Biases, correlations, dispersion indexes and terrain gradient are selected to study the model and experimental data annually and seasonally. Results indicate that WRF simulations show a persistent positive bias in all regions, leading to overestimating CF. In a seasonal analysis, 86% of the CF data falls between the -0.1 and 0.1 bias range. Bias is not related to a physical seasonal phenomenon; instead, it appears to be related to geographic conditions. The findings indicate that different combinations of settings should be chosen to better reflect the geographical conditions and physical phenomena that affect the intricate Mexican landscape for wind energy production. This research identify regions with best reproducibility and suggests potential areas for future research on wind energy forecasting.

Introduction

Mexico's goal of generating at least 35% of its electricity from clean sources by 2024 has led to the need to accelerate the transition to clean energy [1]. This requires solutions to mitigate the variability in renewable energy sources. Mesoscale atmospheric modeling, which numerically resolves regional atmospheric dynamics for short-term forecasting and long-term resource assessment, has been adopted around the world for various weather conditions and latitudes. The Weather Research and Forecasting (WRF) model is an example of a widely used mesoscale model that has been implemented for wind power applications over archipelagos [2,3], tropical regions [4,5], offshore applications [6,7] and complex terrain [8,9].

The spatial resolution of the WRF model is typically set below 10 km and up to 1 km, regardless of the location of the simulated wind fields. Therefore, the model must rely on parameterizations for subgrid physical phenomena that the equations cannot resolve. The choice of parameterizations can have a high degree of freedom, but a common set of parameterizations for studying wind resources in Mexico includes the Kain-Fritsch convection scheme [10], Rapid radiative transfer model (RRTM) long-wave scheme [11], Dudhia short-wave scheme [12], WRF Single Moment 3-class (WSM3) microphysics [13], YonSei University (YSU) parametrization of the boundary layer (PBL) [14], Fifth-Generation Penn State/NCAR Mesoscale Model (MM5) surface layer scheme [15], and Noah land surface model [16], with some variations (Table A.2).

The WRF model has been applied in Mexico for diverse regions and under different study objectives. For example, the Tehuantepec region has the best wind power potential in Mexico [17,18]. In this region, WRF simulations have been implemented to study the effects of model spatial and temporal resolution on wind power production using the parameterizations mentioned above [19,20]. For the Yucatan Peninsula, WRF mesoscale simulations have been useful in determining the main mesoscale and synoptic drivers of wind speed dynamics. During autumn and winter, cold fronts dominate wind variability, and for spring and summer, land-sea breezes are the dominant factors [21,22]. Furthermore, WRF has been used to study wind resources in this region, both offshore and onshore [23].

The Northeast region, with valuable wind power potential [24,25], has been studied with the WRF model to identify the wind power resources in offshore zones [26]. In the northern region of La Rumorosa,

* Corresponding author.
E-mail address: josegus@outlook.com (J.G. Hernandez-Yepes).

https://doi.org/10.1016/j.seta.2024.103848
Received 6 March 2024; Received in revised form 11 May 2024; Accepted 8 June 2024

the WRF model has proven to be valuable in providing information for wind farm operational performance and planning [27]. In the same region, the WRF model has been tested with several parameterizations of the planetary boundary layer (PBL) to fine-tune the wind speed forecasts [28].

In this context, the most popular result in the WRF simulations for the Mexican territory is the Global Wind Atlas (GWA), which uses ERA5, WRF, and Wasp simulations; although these results are publicly available, they are limited to the behavior of the mean wind speeds, which describes the yearly, monthly, or daily wind speeds relative to a climatological reference period [29].

Although mesoscale models have been used to reproduce wind speeds, there is a lack of national-scale analyses that examine wind power generation using high-resolution simulations. One advantage of studying mesoscale wind resources is that they facilitate the application of wind power production. Given its vast size and intricate terrain, Mexico is an ideal location to evaluate the effectiveness of established methods to reproduce wind speed and capacity factors under various physical and meteorological conditions.

In this contribution, we evaluated the ability of WRF simulations to reproduce wind speed conditions and capacity factors at 22 sites, consisting of 30 years of data spread throughout Mexico. Through the analysis of the wind speed and capacity factor, our objective is to evaluate the configuration of the model under different meteorological drivers and under different orographic conditions. From this manuscript, the analysis will provide initial knowledge oriented to understanding the model's capacity to reproduce wind production, recognize its limits in the potential to implement future forecast analysis in regions where the best performance is observed, and identify if parametrizations selected are robust enough to be implemented in the vast and complex Mexican territory from a perspective of wind power production.

The remainder of this paper is organized as follows. Section "Data and Configurations" describes the data used and the configuration of the WRF, Section "Methodology" details the steps developed to compare and analyze the wind speed and the capacity factor, Section "Results and Discussion" presents the results, and Section "Conclusions" presents the conclusions of this study.

Data and configurations

Data measurements

Wind speed measurements are obtained from two sources. The first is from a measurement campaign funded by the United Nations Development Program Global Environmental Finance (UNDP-GEF) and developed by the National Institute of Electricity and Clean Energy (INEEL in Spanish) between 2005 and 2007 [30]. The second source of information is from the Wind Atlas of Mexico project measurement campaign between 2018 and 2020 with seven stations (1NW, 6N, 9NE, 12C, 15TVB, 19T and 21Y) [31].

Wind speeds were measured every second and recorded every 10 min by estimating a representative arithmetic mean. It is important to mention that all 10-min resolution time series were resampled to one hour to agree with the WRF output simulations. A synthesis of the measured heights and completeness at each location is presented in Table 1. Observations were taken at different heights. Additionally, they are extrapolated at 80 m above terrain level using the methodology described in Section "Methodology". Data are considered missing if any measurement height is missing for extrapolation or if the logarithmic extrapolation gives negative values.

Observations are grouped according to geographic conditions, as outlined in prior studies [32]. Additionally, the organization takes into account the height above mean sea level and the terrain gradient, as computed in Section "Methodology".

Geographical conditions

The Northwest region is defined by the Baja California Peninsula, which is bordered by the Cortés Sea and the Pacific Ocean. It extends for approximately 1300 km long and has a width ranging from 45 to 250 km. The region encompasses mountain ranges and deserts, with a rainy season during winter and maximum temperatures with minimum humidity during summer. In this region, wind patterns are influenced by complex interactions between land and sea breezes, seasonal weather patterns, and near-shore environments. The land-sea breezes are associated with thermal contrasts of at least 7 °C between the two surrounding water bodies. Additionally, the complex topography produces a tunneling effect, which directs the wind towards the east [33,34]. Due to its geographical proximity, the 5NW site is aggregated as part of this region, despite not being located in the Baja California Peninsula.

The North region is situated within the Mesa del Norte, extending from the Bravo River in the north to the Zacatecas Mountains in the south. It is bounded by the Sierra Madre Oriental to the east and the Sierra Madre Occidental to the west. The region's topography is characterized by undulating plains at an elevation of approximately 800 to 1000 m above sea level (asl), intersected by mountain ranges reaching 3000 m asl. The MapimíBasin, for instance, is a notable depression that was once a lake but has since become a saline basin. The arid and semi-arid climates prevalent in the region result in high rates of evaporation and limited water runoff, which in turn restricts the presence of large rivers. Desert vegetation is the dominant type of vegetation in this region [35]. The wind patterns in this region are influenced by mid-latitude meteorological systems [36].

The Central region is situated in the Mesa Central, an elevated plateau located in mainland Mexico. It is bordered by the Sierra Madre Oriental to the east, the Sierra Madre Occidental to the west, and the Transvolcanic Belt to the south. The region is characterized by numerous valleys separated from each other by some elevations. The dominant ecosystems are grassland, xerophytic scrub, and mesquite [37]. The temperate climate and fertile soils of this region have facilitated the development of agriculture and human settlements, as evidenced by the presence of some of the most populous cities in the country in this area.

The Northeast region is characterized by a predominantly flat terrain and encompasses the Northern Gulf Coastal Plain. It is bounded by the Sierra Madre Oriental and the Gulf of Mexico, extending from the Rio Bravo to the Transvolcanic Belt. This region is characterized by lowland, sandy, and swampy terrain, with a dry climate. The vegetation is primarily composed of agricultural land, thorny forest, xerophytic scrub, grasslands, and mangrove [38].

The Transvolcanic Belt, so named for the volcanic arc that crosses central-southern Mexico from east to west, is distinguished by its complex terrain features and high altitudes above mean sea level (approximately 90% of the region is located above 1500 m asl). It is 920 km long and serves to divide the Mexican territory from the Pacific Ocean to the Gulf of Mexico. The region is interspersed with wide valleys, plains, and even larger bodies of lakes along its entire length, which results in a high degree of climatic diversity. The vegetation is dominated by various coniferous and oak forests, along with xerophytic scrubland and grasslands [39]. Due to its geographical proximity, the 17TVB site is aggregated as part of this region, despite not being part of the TVB.

The Tehuantepec Isthmus represents the shortest separation in Mexico between the Gulf of Mexico and the Pacific Ocean. It is bounded by the mountains of the Sierra Madre del Sur and the Sierra Madre of Chiapas. This region is covered by tropical vegetation, including jungle, forest, palm groves, grasslands, and swamps [40]. Due to the unique geographical setting and the high pressure systems on the Gulf of Mexico, strong northerly winds flow from the Gulf of Mexico to the

Table 1
Heights above ground level and data availability of measurement stations. Stations are separated and ordered by region: (1–5) Northwest, (6–7) North, (9–10) Northeast, (11–12) Central, (13–17) Center, (18–20) Tehuantepec, and (21–22) Yucatan.

Station	Heights (m)	Months	Years	Completeness (%)	Height asl (m)	Terrain gradient
1NW	20, 40, 60, 80	32	2018–2020	97.62	1343	1206
2NW	20, 40	15	2006–2007	97.28	17	7.39
3NW	15	12	2006	96.22	142	1213
4NW	15	12	2006	98.92	271	3829
5NW	20, 40	12	2006	95.42	11	0.585
6N	20, 40, 60, 80	32	2018–2020	93.92	2131	973
7N	15, 30	14	2006–2007	95.32	1221	2047
8N	16	17	2005	99.9	1499	4155
9NE	20, 40, 60, 80	32	2018–2020	96.79	33	82.8
10NE	20, 40	12	2006	97.87	25	1682
11C	20, 40	12	2007	99.57	2714	949
12C	20, 40, 60, 80	32	2018–2020	76.53	2420	4473
13TVB	10	14	2005–2006	90.53	2546	5724
14TVB	20, 30	12	2005	98.63	2811	6402
15TVB	20, 40, 60, 80	32	2018–2020	94.46	1636	3523
16TVB	20, 40	12	2005	86.21	2332	13,330
17TVB	20, 40	12	2006	97.83	17	0
18T	20, 40	12	2007	97.27	70	2300
19T	20, 40, 60, 80	32	2018–2020	88.89	31	280
20T	20, 40	12	2006	95.41	50	16,583
21Y	20, 40, 60, 80	32	2018–2020	96.78	4	51.5
22Y	20, 40	12	2006	99.75	0	78.4

Pacific Ocean [41]. This region accounts for approximately 60% of the installed capacity of wind energy in Mexico.

The Yucatan region is situated in the Yucatan Peninsula, which is an almost flat region. The calcareous terrain allows rainwater to percolate through, and there are no surface streams, but rather, subterranean waters that have given rise to the formation of cenotes and caves. The vegetation is composed of coastal vegetation, mangrove, low and medium rainforest, savannahs, and petenes [42]. Wind in this region experiences influences from land-sea breezes and large-scale circulations [32,43].

A portion of the description of the above mentioned regions was taken from [37,44].

Mesoscale model configurations

The Weather Research and Forecasting (WRF) model version 4.3 is a mesoscale model that resolves the nonhydrostatic compressible Euler equations [45]. In this work, the simulations are run individually for each site with a single configuration with resolutions of 25 km, 5 km, and 1 km (Fig. 1(b)). WRF simulations are initialized every 24 h and run for 30 h, with 6 h of spin-up, which are then discarded.

The ERA5 reanalysis [46,47] is used as input to specify both lateral boundary conditions and initial conditions, with a horizontal resolution of approximately 30 km and 137 vertical levels. The lateral boundary conditions are ingested every 6 h. The parameterizations used are the same as in [19].

WRF simulations cover the same time spans as observations (Table 1). In total they sum more than 34 years of data.

Methodology

To evaluate the capability of the WRF model to reproduce wind speeds and capacity factor, modeled gridded data and observations are processed to obtain a time series of wind speeds equal as the height of the Vestas V90, which is 80 m above ground. Thus, the models' data at the highest resolution (1 km) are first interpolated bilinearly and then interpolated vertically. The interpolation in the vertical direction is done using two values: one at 10 m and the other at an estimated second model level of approximately 86 m, which was calculated by converting the geopotential height to geometric height. The wind speeds of the virtual hub height are obtained using a power law method; when there are two heights the shear exponent is calculated using the power law equation and solving for α (equation in Appendix "Supporting information") and for four stations with one height we consider a shear exponent of 1/7 [48].

To evaluate similarities in behavior between stations, the results are classified into regions following the classification delimited in Fig. 1(a).

The first analysis compares the cumulative distribution functions of the wind speed data sets using the Kolmogorov–Smirnov D_n statistic

$$D_n = \max_x(|F_o(x) - F_m(x)|), \tag{1}$$

where F_o is the cumulative distribution function of observations, F_m is the cumulative distribution function of model data, and n is the total number of samples [49]. The value of the Kolmogorov–Smirnov test can range from 0 to 1. The closer the value is to 0, the more similar the distributions of observed and simulated wind speeds are. A direct visual comparison is also made between experimental and modeled data. These two criteria will provide elements for studying the simulation of observed wind in statistical terms.

Afterwards, we assessed the correlation and errors of wind speeds and capacity factors. To carry out the study, we chose Pearson's correlation coefficient

$$r = \frac{\sum_{i=0}^{n-1}(m_i - \overline{m})(o_i - \overline{o})}{\sqrt{\sum_{i=0}^{n-1}(m_i - \overline{m})^2}\sqrt{\sum_{i=0}^{n-1}(o_i - \overline{o})^2}}, \tag{2}$$

the centered root mean square difference

$$CRMSD = \sqrt{\frac{1}{n}\sum_{i=0}^{n-1}((m_i - \overline{m}) - (o_i - \overline{o}))^2}, \tag{3}$$

and the standard deviation, all displayed on Taylor graphs. Here, m is the model value and o is the observed value. Taylor diagrams are normalized to compare different sets of data.

Afterwards, wind speed data are used to estimate the capacity factor (CF) by evaluating the values with a power curve (Fig. A.8). Capacity factor is defined as the ratio of the energy production of the wind turbine to the energy that could have been produced if it operated at rated power over a given time period. Its formula is given in the Appendix "Supporting information".

An analysis of annual CF distribution is performed. Also, the mean values of CF of observed wind speeds are compared against the mean values of CF of modeled wind speed.

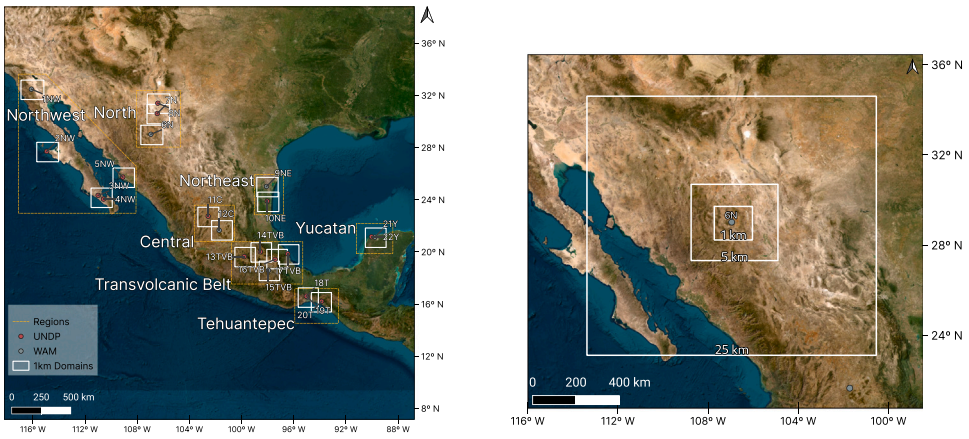

(a) Masts locations (b) Nesting

Fig. 1. (a) Sites with measurements clustered by regions in orange. White rectangles represent the innermost domain of WRF simulations for each site. (b) Example of domain nesting configuration for site 6N. Each location has a similar nesting configuration of domains.

The next analysis compares three parameters: (1) the gradient of the surrounding terrain height as a measure of terrain complexity, (2) the K-S index and (3) the correlation coefficient. The goal is to determine a relationship between the complexity of terrain and the performance of simulations. The magnitude of gradient of the terrain height above mean sea level $\|\nabla h\|$ is obtained as:

$$\|\nabla h\| = \sqrt{\left(\frac{\partial h}{\partial x}\right)^2 + \left(\frac{\partial h}{\partial y}\right)^2}, \tag{4}$$

where h is the height above mean sea level, x is the longitudinal direction and y is the latitudinal direction. The mean and the standard deviation are obtained for the five nearest grid points to each station location.

The final part of the study focuses on the seasonal dependence of the results. To assess it the mean values of each site are calculated by season. Sites with more than one year of data consider the mean value along the years. Seasons are defined as winter (December, January and February), spring (March, April, May), summer (June, July, August) and autumn (September, October, November).

We estimate the mean bias error ($bias$) and the mean absolute error (MAE) of the wind speed and CF for each station and season; equations are shown in the Appendix "Supporting information". Finally, the bias of all seasons and sites are grouped to analyze its behavior both overall and seasonally.

Results and discussion

Reproduction of wind speed distributions

The first analysis is to compare wind speed distributions of wind speed of observations against WRF simulations. Locations with low K-S values (<0.1) are observed in the Northeast, Central, Yucatan and a portion of the Transvolcanic Belt (TVB) region (13TVB, 14TVB and 15TVB). On the contrary, the Tehuantepec region and sites 4NW, 5NW, 8N, 16TVB and 17TVB have a K-S value greater than 0.1 (see Fig. 2(b)). In Fig. 2(a) the experimental and modeled histograms are presented in color and black line, respectively. Histograms for the Tehuantepec region indicate an overestimation of higher wind speeds, which could be the cause of the higher K-S index values for these locations. This effect is also seen, although to a lesser degree, in locations with a K-S index greater than 0.1.

The histograms and the K-S index reveal a diverse degrees of accuracy in the reproduction of wind speed distributions. While some regions are clearly well reproduced (Northeast and Central) other regions are reproduced with mixed results (Northwest and Transvolcanic Belt) and others with poor accuracy (Tehuantepec). A clear example of poor reproduction of wind speed is the 20T site which fail to reproduce the bimodal distribution characteristic of this region [50].

Wind speed and CF error metrics

Linear correlation and dispersion parameters are presented in Taylor's diagram for each station (Figs. 3 and A.9). Diagrams of all regions are shown in Appendix "Supporting information". Results are divided by region, and to assess how these indicators vary between wind speeds and CF estimations, both values are presented in black and yellow, respectively. A red line is also included to delimit values above or below the 0.7 correlation coefficient.

The CF calculation process impacts $CRMSD$ and the correlation to different degrees depending on the region. Wind speeds in Northeast stations exhibit high correlations (Fig. 3(a)). This pattern is maintained when the CFs are calculated in this region, but the variability decreases. In contrast, the Transvolcanic Belt region exhibits low correlations (Fig. 3(b)). For instance, the 15TVB site located in the Transvolcanic Belt region has the highest standard deviation and CRMSD values. For the CF calculations in this region, the degree of errors and correlations persist as in wind speed estimations.

In the Northwest region, there is a clear cluster of stations indicating a well-defined area in terms of CRMSD and correlation (Fig. A.9(a)). For the North region correlations are similar between wind speed and CF data; however, a larger dispersion is observed in the 6N and 7N stations (Fig. A.9(b)).

The Central and Yucatan regions exhibit a similar pattern, with correlation, standard deviation, and CRMSD values that remain consistent between the wind and CF variables (Figs. A.9(c), and A.9(e) respectively). In the Tehuantepec region A.9(d), when wind speeds are compared, all stations begin to be highly correlated with greater variability. Once CF was estimated, normalized standard deviation and correlations were 1 and 0.7 respectively.

For the locations studied, the Pearson correlation coefficient ranges from 0.53 to 0.89 3. High correlations in wind speed are observed in the Northeast and Tehuantepec regions. However, in the Tehuantepec region after estimating the CF the correlations are now close to the 0.7 value. Only in the Northeast region remain high correlations in CF. Regular correlations are present in the Central region (around 0.7) for both wind speed and CF, along with 1NW, 16TVB, and 22Y. Finally, low correlations (around 0.5 and 0.6) appear for the North,

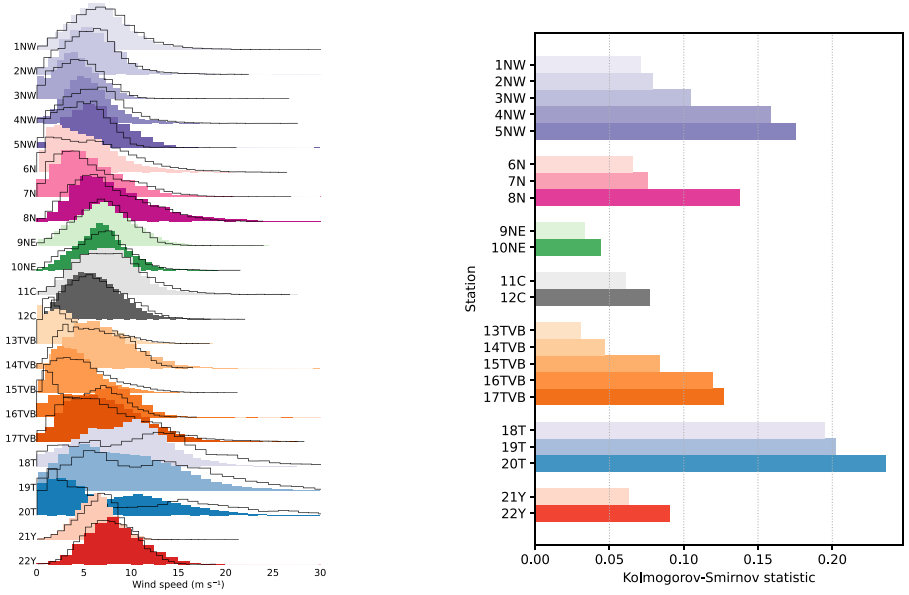

(a) Histograms (b) Kolmogorov-Smirnov

Fig. 2. (a) Distributions of wind speed observations in color and WRF data in black line. (b) Kolmogórov-Smirnov statistics for wind speed distributions of observations and models.

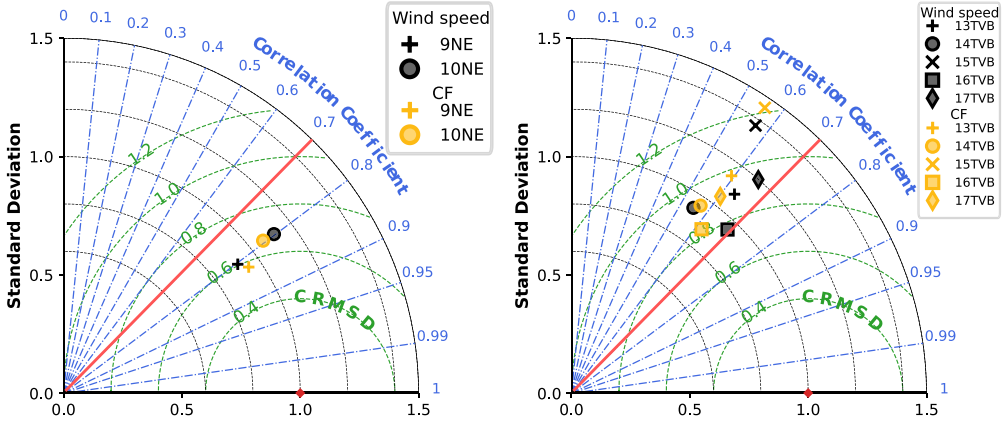

(a) Northeast (b) Transvolcanic Belt

Fig. 3. Relationship of CRMSD, standard deviation, and correlation coefficient: examples of good correlation (>7) and low CRMSD (~0.6) (Northeast region); and low correlation (<7) and high CRMSD (>0.8) (Transvolcanic Belt region). In black, indicators for wind speed are plotted, and in yellow, for CF. The red line marks the boundary between good and poor correlations delimited by a 0.7 Pearson correlation coefficient.

Northwest, and Transvolcanic Belt regions. In summary, for most of the stations, the wind speed has a higher correlation than the CF. In the Appendix "Supporting information", examples of good, regular and bad correlations are presented in Figs. A.10(a), A.10(b), and A.10(c), respectively.

In general, regional clusters demonstrate the varying behavior of stations, which implies that the regional diversity approach should be considered when conducting a mesoscale analysis. The model's settings used resulted in higher correlations in the Northeast region, followed by the Central and Tehuantepec regions, where correlations were estimated between 0.7 and 0.8. It is important to mention that Tehuantepec and Northeast concentrate the most installed capacity of the country.

Accuracy of capacity factor calculations

Now we analyze the CF values by looking at the violin plot in Fig. 4. The CF calculated using WRF wind speed are shown in orange and the CF calculated using observations are shown in blue. In the entire Northwest region the capacity factor is overestimated, excluding the 5NW station. The North region has large deviations in 6N and 7N, whereas 8N shows better agreement in terms of the CF distribution. In the Northeast, 9NE has a negative bias and 10NE a positive bias, but both have a similar reproduction of the wind speed distribution as observations. Like most of the stations, CF of the Central region is overestimated. In the Transvolcanic Belt region, CF is reproduced with different biases. In Tehuantepec, CF is consistently overestimated. Finally, the Yucatan region shows good reproduction of CF distribution with mixed bias.

CF calculations are expected to be better correlated due to the effect of the power curve, which may filter out wind speed data to map it into a CF distribution. However, as seen in Section "Wind speed and CF error metrics" in most cases the effect of CF calculation is higher error statistics due to the non-linearity of the power curve. Therefore, slight variations in wind speed will be reflected in high variations in

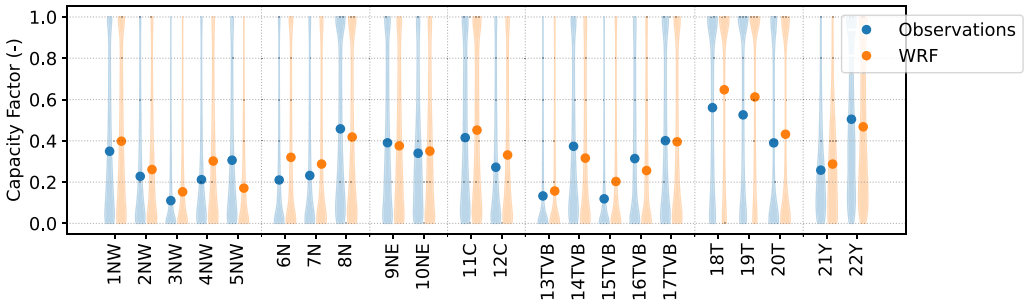

Fig. 4. Violin plots represent the kernel density estimations for the distributions of capacity factors or each station, results are grouped by regions. Points indicate mean values. In blue are presented the estimations using experimental data and in orange estimation using WRF data.

the CF. Furthermore, biases in wind speed distributions are reflected in CF distributions.

Orography relationship

In this section the relationship between three parameters is analyzed by region: (1) the K-S index obtained in Section "Reproduction of wind speed distributions", (2) the correlation coefficient obtained in Section "Wind speed and CF error metrics" and the gradient of the terrain height. Illustrations are presented as part of Appendix "Supporting information".

The Northwest region, exhibits correlation coefficients ranging from 0.6 to 0.7, regardless of terrain location or gradient (Fig. A.11(a)). Sites with high terrain gradients (1NW, 4NW) (complex terrain), as well as those located in flat areas (coastal zones) such as 5NW and 2NW, all encounter difficulties in achieving accurate reproductions.

In the North region, sites featuring medium to high terrain gradients (~3400) exhibit low correlations (<0.6) (Fig. A.11(b)). Despite all stations displaying correlations below 0.7, they demonstrate a medium to low K-S index (<0.16), indicating a well-reproduced wind speed distribution.

The Northeast region, has well correlated wind speeds (~0.8). Moreover, a low K-S index indicates an effective reproduction of wind speed distribution in this region (Fig. A.11(c)).

In the Central region the reproduction of wind speed does not seem to be influenced by the terrain gradient, with well correlated wind speeds (~0.8) and a low K-S value, indicative of accurate wind speed distribution reproduction (Fig. A.11(d)).

In the Transvolcanic Belt region all sites have correlation coefficients of 0.7 or lower (Fig. A.11(e)). Remarkably, the 16TVB station, despite a high gradient, exhibits the highest correlation coefficient.

The Tehuantepec region sites exhibit high correlation coefficients, but they do not accurately reproduce the wind speed distribution (Fig. A.11(f)). It is important to note that the correlation coefficient remains constant regardless of the terrain gradient.

In the Yucatan region simulated wind speeds show moderate correlations (~0.7) with well reproduced distributions (Fig. A.11(g)).

Based on these findings, it is evident that the WRF mesoscale model proves valuable in accurately replicating wind dynamics within flat terrain, as highlighted in the Northeast and Central regions. However, challenges arise when dealing with complex terrains, except notably in the correlation in the Tehuantepec region. The varying performance observed in the Trans Volcanic Belt region emphasizes the need for caution when using the WRF model to areas with intricate topographical features.

In general, while simulations of wind speed are accurate in flat areas where wind speed tends to be low, they present challenges in complex terrain, typically at higher elevations. However, at complex terrains, wind speed simulations are significant for wind power generation due to higher wind speeds. This reveals an area of opportunity for future works related to numerical modeling and wind resource assessment.

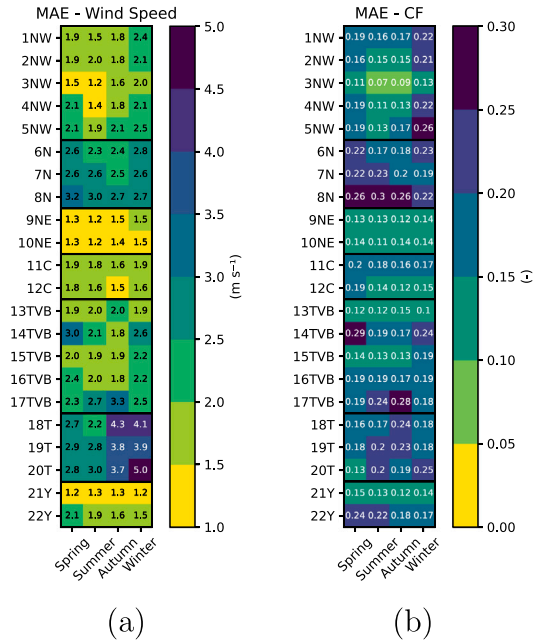

Fig. 5. Heatmap of seasonal MAE of wind speed (a), and of CF (b).

Moreover, results reveal potential limitations in the model's ability to accurately reproduce wind speeds in coastal regions. This is particularly evident in the Northwest and Yucatan regions, suggesting that proximity to coastlines may pose challenges for the WRF model in achieving precise wind speed distribution reproduction.

Seasonal analysis

In the preceding sections, the annual behavior of error metrics and distribution was studied, and now we will look into the effect of seasonality on the model for each site. This section will concentrate on the seasonal analysis of the modeled wind speeds and CF in terms of seasonal bias and MAE. Figs. 5 and 6 show MAE and bias respectively, of wind speeds and CF estimates for each station and region on the seasonal scale.

The errors of the stations vary according to the region. In general, capacity factor calculations have a high degree of error, from 10% to 30%. The Northeast and Yucatan regions have the lowest MAE values. The Transvolcanic Belt and Northwest regions have a mix of regular MAE values. The Tehuantepec region has significantly higher MAE values in winter and autumn compared to spring and summer (as seen in Fig. 5-a). Moreover, the level of errors in wind speed is transferred to the CF. Clear examples are the North and Northeast regions (Fig. 5-b).

WRF simulations tend to overestimate the wind speed in most of the stations, which also leads to an overestimation of the CF; this is

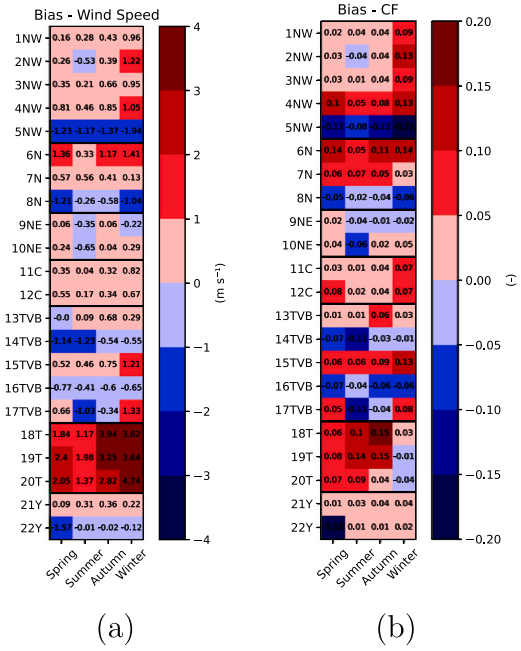

Fig. 6. Heatmap of seasonal bias of wind speed (a) and bias of CF (b).

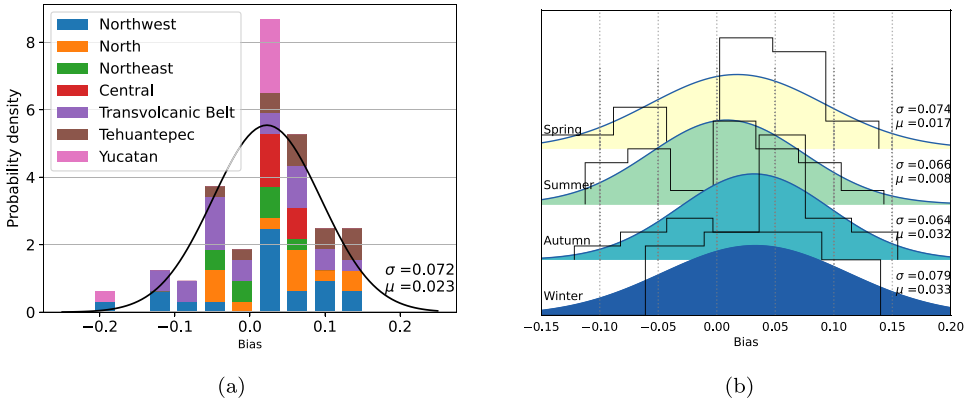

Fig. 7. Distribution of bias by location (a) and during seasons (b). The black line in (a) represent a fitted normal probability density function. The colored Gaussian bells in (b) represent normal probability density functions per season.

observed in abundant positive values of bias (Fig. 6). Regardless of the season, the wind speed and CF in the Northwest and North regions are consistently overestimated, except for the 5NW and 8N stations. The Northeast region shows a mixed pattern, but with small biases. Wind speeds and CF in the Transvolcanic Belt region have a diverse behavior with 14TVB and 16TVB showing persistent underestimations. It should be noted that this region is characterized by intricate topography.

During autumn and winter, wind speed is highly overestimated in the Tehuantepec region; however, the CF is underestimated in the same season, and this is associated with the wind turbine cut wind speed. Finally, the Yucatan region shows a consistent pattern of bias for wind speed and CF.

To identify whether the magnitude of the bias is related to seasonal effects or regional factors, seasonal bias was estimated for all sites and plotted on histograms based on two criteria: their presence per location (see Fig. 7(a)) and by season (see Fig. 7(b)). Regarding the location categorization, the mean of bias is 0.02, and the standard deviation is 0.07, indicating a positive bias. WRF simulations provided the most precise depiction of the Central and Northeast regions, with a bias ranging from −0.1 to 0.1. Taking into account all regions, the configuration along with the parameterizations used generated seasonal representations with biases in the same range, which represented 86.4% of all simulated seasons. The findings demonstrate that the chosen settings and parameterizations generally do a commendable job of reproducing wind conditions. The behavior of regional bias displays two patterns: regions with clustered bias values, such as the Northeast (shown in green 7(a)), which may suggest a well-represented area; and regions with dispersed bias values, such as the Transvolcanic Belt region, where negative biases are also present. This outcome implies that areas with broader bias values may necessitate additional examination to enhance mesoscale simulations. In Fig. 7(b) seasonal biases are grouped by seasons; in general, seasonal distributions show mean values between 0.01 and 0.03, with similar standard deviations. These seasonal distributions (Fig. 7(b))are comparable to the distribution of bias of all regions categorized by location (Fig. 7(a)), suggesting that the presence of bias is not affected by the season. However, the bias in the various locations varies in magnitude, suggesting that bias is influenced by the geography of each region rather than by season of the year.

Errors and biases in wind speed simulations exhibit considerable variability across regions. These discrepancies in wind speeds are reflected in the results of CF calculations. However, the values estimated by CF exhibit a notable decline compared to the original simulations.

The variation in bias by location and across different seasons suggests that a regional approach is necessary to avoid generalizing the performance of simulations. Therefore, further studies should prioritize investigating geographical parameters, such as orography and land use, in order to gain more accurate simulations.

Conclusions

This study assesses the ability of the WRF mesoscale model to simulate wind speeds and capacity factors in various regions of Mexico. Wind speeds at twenty-two sites were modeled at a horizontal resolution of 1 km and compared with data from two measurement campaigns. The analysis was carried out by comparing distributions, estimating wind speeds and CF error metrics, and finally their relation with the terrain gradient.

Our analysis of wind speed distributions, using the K-S index, in various regions of Mexico indicates that the WRF model exhibits a degree of precision that varies throughout the country. Northeast, Yucatan, and Central show well-reproduced distributions. The Tehuantepec region shows the highest K-S values, probably due to overestimations of the high wind speeds. The Northwest and Transvolcanic Belt regions exhibit mixed results. In general, only 22% of the locations showed K-S values above 0.1.

Estimating the capacity factor is a crucial step that can result in differences between predicted and real values, stemming from the nonlinear nature of the wind turbine power curve. Only three of the 22 cases studied resulted in CF below 20%, indicating an abundant wind resource in all regions. NE region showed the best similarity among the regions. Tehuantepec and Central regions showed a persistent overestimation of CF. However, the errors maintain consistent values for wind speeds and capacity factors. In a seasonal analysis, 86% of the CF data falls between the −0.1 and 0.1 bias range.

From an annual perspective, 60%, the WRF simulations show a positive bias, 22% presents an underestimate, and similar values were observed in the remaining 18%. This bias is unaffected by seasonal changes; thus, bias is mainly dominated by the geographical features of the region.

The preceding findings indicate the need for a regionally diverse approach when performing a mesoscale analysis. The results demonstrate that there are areas of high performance, namely Northeast, Central, and Yucatan, while there are also areas of regular to low performance, specifically the Northwest, North, and Transvolcanic Belt. This suggests potential areas to prioritize to improve knowledge for wind power forecasting in Mexico.

Mesoscale modeling is a valuable tool for studying wind speeds for energy production. This analysis provided valuable information to dissect various Mexican conditions. The best modeled regions are well known for their abundant resources; therefore, further analysis can be conducted on specific regions incorporating parametrizations and static data with better geographic inputs.

CRediT authorship contribution statement

J.G. Hernandez-Yepes: Writing – original draft, Visualization, Validation, Software, Methodology, Investigation, Formal analysis, Data curation, Conceptualization. **O. Rodriguez-Hernandez:** Writing – review & editing, Supervision, Resources, Project administration, Methodology, Investigation, Funding acquisition, Formal analysis, Conceptualization. **C.A. Lopez-Villalobos:** Writing – review & editing, Visualization, Software, Methodology, Formal analysis, Conceptualization. **O. Martínez-Alvarado:** Writing – review & editing, Supervision, Methodology, Conceptualization.

Declaration of competing interest

The authors declare that they have no known competing financial interests or personal relationships that could have appeared to influence the work reported in this paper.

Data availability

The data supporting the findings of this study can be accessed through the following link: https://github.com/heyej/Mexico-WRF-wind-speed. While the majority of the data is included, due to size constraints, some datasets may be provided upon direct inquiry to the corresponding author.

Acknowledgments

Funding

This work was supported by Mexico CONACYT-SENER Sustentabilidad Energética (Institutional Strengthening for Energy Sustainability) “Strengthening of the field of Wind Energy in the Doctoral Program in Engineering Field of Knowledge in Energy based in the Institute of Renewable Energies of the National Autonomous University of Mexico”[grant number 272063], José Gustavo Hernández-Yepes PhD CONACyT National Postgraduate Scholarship. The authors thank M.I. Kevin Alquicira Hernández for his technical support and administration of computational service.

Thanks to M.I. Diego Canul Reyes for his guidance with python and illustrations.

Appendix. Supporting information

A.1. Tables

See Table A.2.

A.2. Formulae

- Shear exponent is calculated as

$$\alpha = \frac{\log\left(\frac{u_h}{u_l}\right)}{\log\left(\frac{z_h}{z_l}\right)} \tag{.1}$$

where u_h and u_l are the wind speed at the high level and the low level respectively, and z_h and z_l are the heights above ground level at high level and at low level respectively.

- Equations of the bias error and mean absolute error:

$$Bias = \frac{1}{N}\sum_{i=1}^{N}(x_{m,i} - x_{o,i}) \tag{.2}$$

$$MAE = \frac{1}{N}\sum_{i=1}^{N}|x_{m,i} - x_{o,i}| \tag{.3}$$

where $x_{m,i}$ and $x_{o,i}$ are the ith data of model and observations, respectively.

- CF is calculated as

$$CF = \sum_{i=1}^{N}\frac{P(u_i)\Delta T}{P_R} \tag{.4}$$

where N are the data points of the wind speed time series (u) sampled at intervals Δt, P_R is the rated power and T is the total calculation time.

A.3. Figures

See Figs. A.8, A.9, A.10 and A.11.

Table A.2
Literature review of works that use the same schemes or parametrizations to simulate wind resources in Mexico.

	Kain-Fritsch convection	RRTM long-wave	Dudhia short-wave	WSM3 microphysics	YSU PBL	MM5 surface layer	Noah land surface model
Acs et al. [51]	✓	✓	–	✓	✓	–	✓
Allende-Arandía et al. [43]	✓	✓	✓	–	✓	–	✓
Hernández-Yepes et al. [19]	✓	✓	✓	✓	✓	✓	✓
Lopez-Villalobos et al. [20]	✓	✓	✓	–	✓	✓	✓
Lopez-Espinoza et al. [52]	✓	✓	✓	✓	✓	–	–
Allende-Arandía et al. [21]	✓	✓	✓	✓	✓	✓	✓
Diaz-Esteban et al. [53]	✓	✓	✓	–	✓	✓	✓
Pereyra-Castro et al. [28]	✓	✓	✓	✓	✓	–	✓

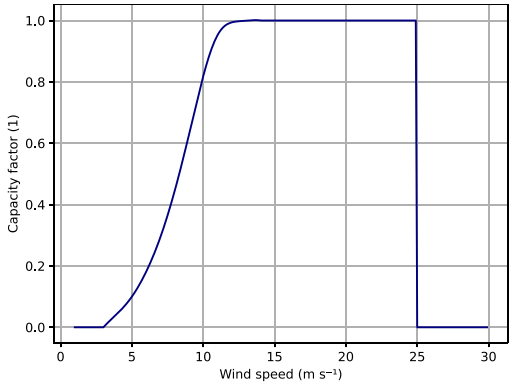

Fig. A.8. Normalized power curve of 2 MW Vestas V90. Wind speed cut-in occurs at 3 ms^{-1} and cut-out occurs above 25 ms^{-1}.

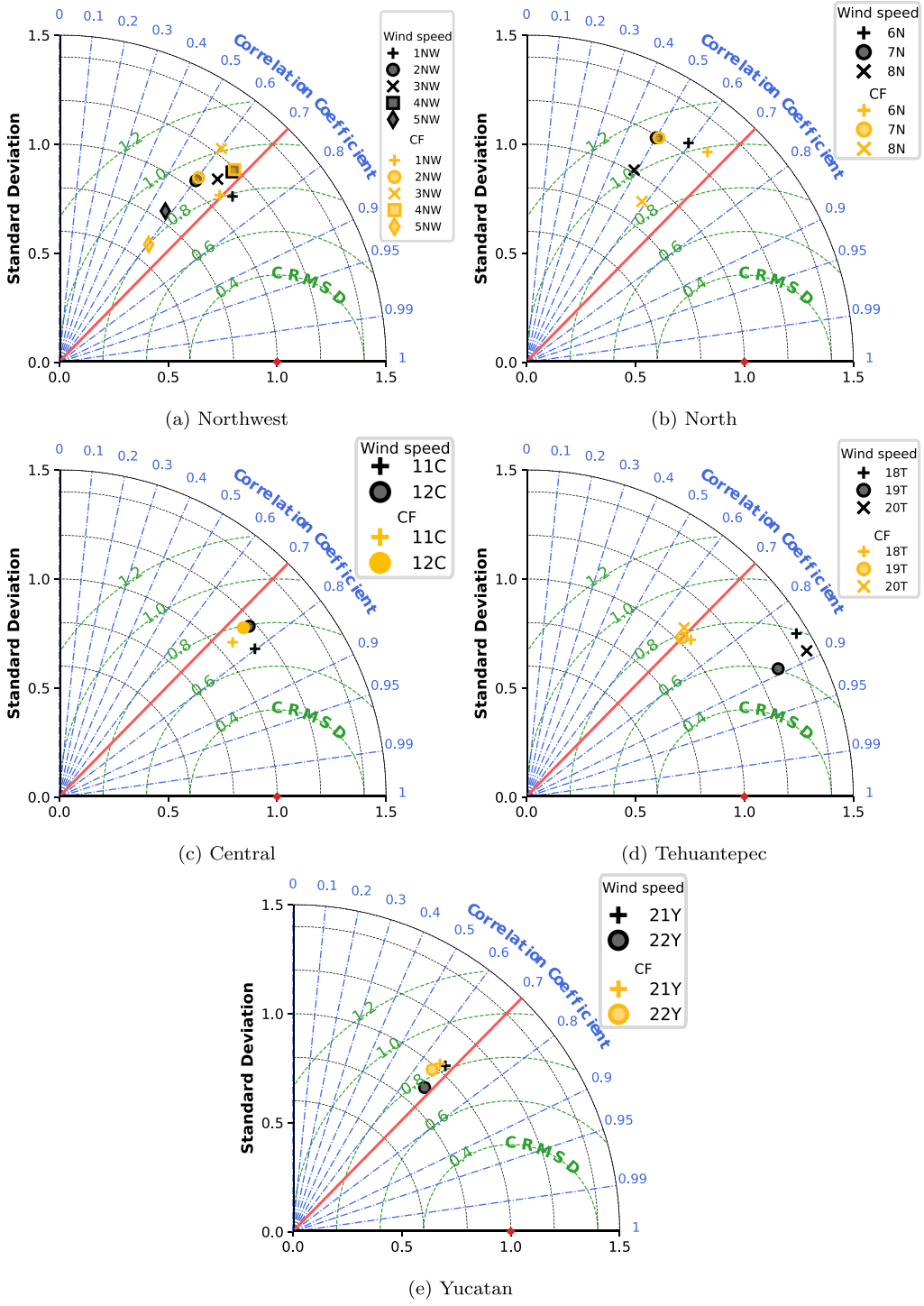

Fig. A.9. Relationship of CRMSD, standard deviation, and correlation coefficient. Results are presented per region; in black, indicators for wind speed are plotted, and in yellow, for CF. The red line marks the boundary between good and poor correlations delimited by a 0.7 Pearson correlation coefficient.

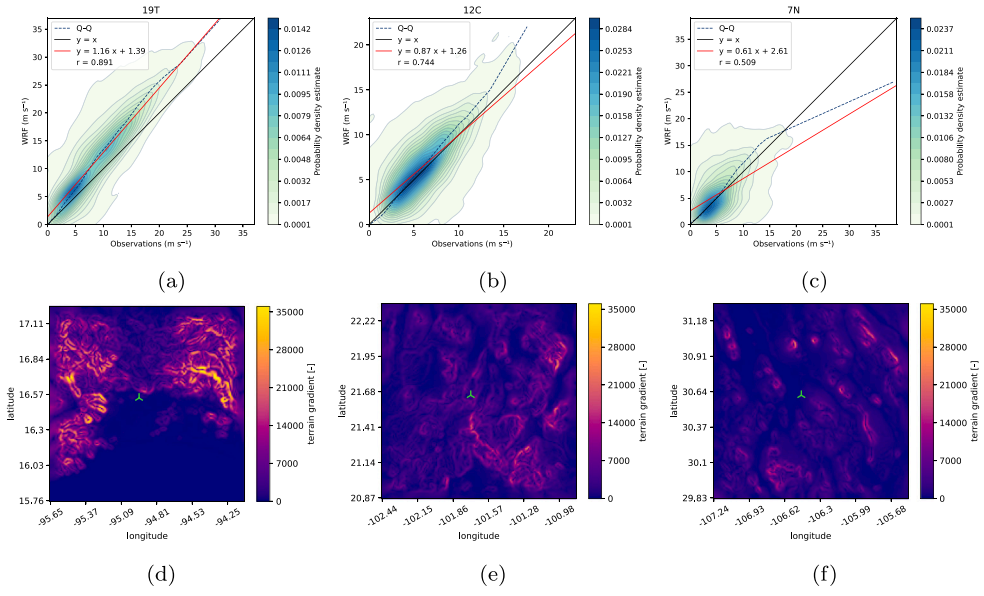

Fig. A.10. Figures at the top present the density plot of wind speeds for different correlation cases: (a) 19T - high correlation, (b) 12C - regular correlation, (c) 7N - low correlation. The figures at the bottom illustrate the terrain gradient of the 1 km domain of the same locations as the figures at the top. The locations of the measurement stations are marked in green.

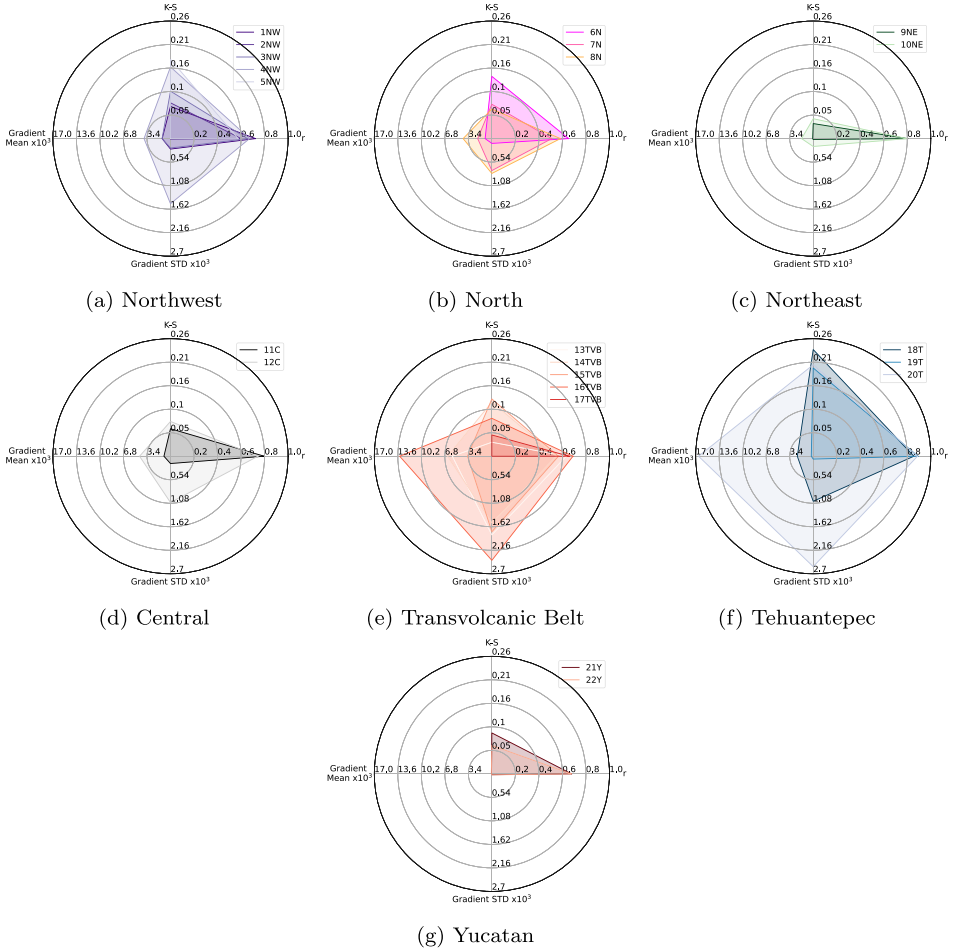

Fig. A.11. Relationship of the performance of simulations with the terrain gradient. The spider plots relate the K-S index, the correlation coefficient, the mean of the terrain gradient and its standard deviation.

References

[1] Bracho R, Alvarez J, Aznar A, Brancucci C, Brinkman G, Cooperman A, Flores-Espino F, Frazier W, Gearhart C, Fernández OJG, Hurlbut D, Kolker A, Kroposki B, Lantz E, Maclaurin G, Roberts B, Lankao PR, Saur G, Stark G, Sky H. Mexico clean energy report. 64. http://dx.doi.org/10.2172/1862951.

[2] Dayal KK, Bellon G, Cater JE, Kingan MJ, Sharma RN. High-resolution mesoscale wind-resource assessment of Fiji using the weather research and forecasting (WRF) model. Energy 2021;232:121047. http://dx.doi.org/10.1016/j.energy.2021.121047.

[3] Argüeso D, Businger S. Wind power characteristics of Oahu, Hawaii. Renew Energy 2018;128:324–36. http://dx.doi.org/10.1016/j.renene.2018.05.080.

[4] Perini de Souza NB, Sperandio Nascimento EG, Bandeira Santos AA, Moreira DM. Wind mapping using the mesoscale WRF model in a tropical region of Brazil. Energy 2022;240:122491. http://dx.doi.org/10.1016/j.energy.2021.122491.

[5] Gil Ruiz SA, Cañón Barriga JE, Martínez JA. Assessment and validation of wind power potential at convection-permitting resolution for the Caribbean region of Colombia. Energy 2022;244:123127. http://dx.doi.org/10.1016/j.energy.2022.123127.

[6] Ghafarian P, Mohammadpour Penchah M. Wind resource assessment over the Persian gulf and Oman Sea using a numerical model simulation and satellite data. J Ocean Eng Mar Energy 2023. http://dx.doi.org/10.1007/s40722-022-00273-8.

[7] Salvação N, Guedes Soares C. Wind resource assessment offshore the Atlantic Iberian coast with the WRF model. Energy 2018;145:276–87. http://dx.doi.org/10.1016/j.energy.2017.12.101.

[8] Guevara Luna MA, Casallas A, Belalcázar Cerón LC, Clappier A. Implementation and evaluation of WRF simulation over a city with complex terrain using Alos-Palsar 0.4 s topography. Environ Sci Pollut Res 2020;27(30):37818–38. http://dx.doi.org/10.1007/s11356-020-09824-8.

[9] Carvalho D, Rocha A, Gómez-Gesteira M, Santos C. A sensitivity study of the WRF model in wind simulation for an area of high wind energy. Environ Model Softw 2012;33:23–34. http://dx.doi.org/10.1016/j.envsoft.2012.01.019.

[10] Kain JS. The kain–fritsch convective parameterization: an update. J. Appl. Meteorol. 2004;43:170–81. http://dx.doi.org/10.1175/1520-0450(2004)043<0170:TKCPAU>2.0.CO;2.

[11] Mlawer EJ, Taubman SJ, Brown PD, Iacono MJ, Clough SA. Radiative transfer for inhomogeneous atmospheres: RRTM, a validated correlated-k model for the longwave. J Geophys Res: Atmos 1997;102(D14):16663–82. http://dx.doi.org/10.1029/97JD00237.

[12] Dudhia J. Numerical study of convection observed during the winter monsoon experiment using a mesoscale two-dimensional model. J. Atmosp. Sci. 1989;46(20):3077–107. http://dx.doi.org/10.1175/1520-0469(1989)046<3077:NSOCOD>2.0.CO;2.

[13] Hong S-Y, Dudhia J, Chen S-H. A revised approach to ice microphysical processes for the bulk parameterization of clouds and precipitation. Mon. Weather Rev. 2004;132:103–20. http://dx.doi.org/10.1175/1520-0493(2004)132<0103:ARATIM>2.0.CO;2.

[14] Hong S-Y, Noh Y, Dudhia J. A new vertical diffusion package with an explicit treatment of entrainment processes. Mon Weather Rev 2006;134(9):2318–41. http://dx.doi.org/10.1175/MWR3199.1.

[15] Jiménez PA, Dudhia J, González-Rouco JF, Navarro J, Montávez JP, García-Bustamante E. A revised scheme for the WRF surface layer formulation. Mon Weather Rev 2012;140(3):898–918. http://dx.doi.org/10.1175/MWR-D-11-00056.1.

[16] Chen F, Dudhia J. Coupling an advanced land surface–hydrology model with the penn state–NCAR MM5 modeling system. Part I: Model implementation and sensitivity. Mon Weather Rev 2001;129(4):569–85. http://dx.doi.org/10.1175/1520-0493(2001)129<0569:CAALSH>2.0.CO;2.

[17] Hernández-Escobedo Q, Manzano-Agugliaro F, Zapata-Sierra A. The wind power of Mexico. Renew Sustain Energy Rev 2010;14(9):2830–40. http://dx.doi.org/10.1016/j.rser.2010.07.019.

[18] Lopez-Villalobos C, Martínez-Alvarado O, Rodriguez-Hernandez O, Romero-Centeno R. Analysis of the influence of the wind speed profile on wind power production. Energy Rep 2022;8:8079–92. http://dx.doi.org/10.1016/j.egyr.2022.06.046.

[19] Hernández-Yepes JG, Rodríguez-Hernández O, Martínez-Alvarado O, Magaldi-Hermosillo AV, Drew D. Influence of spatial resolution in mesoscale modeling to reproduce wind power production in southern Mexico. J Renew Sustain Energy 2022;14(4):043303. http://dx.doi.org/10.1063/5.0091384.

[20] Lopez-Villalobos C, Rodriguez-Hernandez O, Martínez-Alvarado O, Hernandez-Yepes J. Effects of wind power spectrum analysis over resource assessment. Renew Energy 2020;167:761–73. http://dx.doi.org/10.1016/j.renene.2020.11.147.

[21] Allende-Arandía ME, Zavala-Hidalgo J, Torres-Freyermuth A, Appendini CM, Cerezo-Mota R, Taylor-Espinosa N. Sea-land breeze diurnal component and its interaction with a cold front on the coast of Sisal, Yucatan: A case study. Atmos Res 2020;244:105051. http://dx.doi.org/10.1016/j.atmosres.2020.105051.

[22] Cahuich-López MA, Mariño-Tapia I, Souza AJ, Gold-Bouchot G, Cohen M, Valdés-Lozano D. Spatial and temporal variability of sea breezes and synoptic influences over the surface wind field of the Yucatán Peninsula. Atmósfera 2020;33(2):123–42. http://dx.doi.org/10.20937/ATM.52713.

[23] García-Caballero E, Appendini CM, Figueroa-Espinoza B, Allende-Arandía ME, Magar V, Gross MS. Wind energy potential assessment for Mexico's Yucatecan Shelf. Energy Sustain Dev 2023;74:415–29. http://dx.doi.org/10.1016/j.esd.2023.04.016.

[24] Perea-Moreno A-J, Alcalá G, Hernandez-Escobedo Q. Seasonal wind energy characterization in the gulf of Mexico. Energies 2020;13(93). http://dx.doi.org/10.3390/en13010093.

[25] Salgado-Herrera NM, Campos-Gaona D, Anaya-Lara O, Robles M, Rodríguez-Hernández O, Rodríguez-Rodríguez JR. THD reduction in distributed renewables energy access through wind energy conversion system integration under wind speed conditions in tamaulipas, Mexico. Energies 2019;12(3550). http://dx.doi.org/10.3390/en12183550.

[26] Meza-Carreto J, Romero-Centeno R, Figueroa-Espinoza B, Moreles E, López-Villalobos C. Outlook for offshore wind energy development in Mexico from WRF simulations and CMIP6 projections. Energies 2024;17(1866). http://dx.doi.org/10.3390/en17081866.

[27] Cuevas-Figueroa G, Stansby PK, Stallard T. Accuracy of WRF for prediction of operational wind farm data and assessment of influence of upwind farms on power production. Energy 2022;254:124362. http://dx.doi.org/10.1016/j.energy.2022.124362.

[28] Pereyra-Castro K, Caetano E, Altamirano del Razo D. WRF wind forecast over coastal complex terrain: Baja California Peninsula (Mexico) case study. Arab J Geosci 2021;14(19):1972, doi:10/gn6qgw.

[29] Olsen BT, Hahmann AN, Cavar D, Peña A, Villanueva H, Davis NN, Hansen JC. Mesoscale and microscale downscaling for the Wind Atlas of Mexico (WAM) project. DTU Wind Energy 2021;(E-0223):77.

[30] UNDP. Plan de acción para eliminar barreras para la implementación en gran escala de la energía eólica En México. Tech. rep., México: UNDP; 2012.

[31] Villanueva H, Peña A, Hansen JC. Wind Atlas for Mexico (WAM) observational wind atlas. Tech. rep. E-0224, Risø, Roskilde, Denmark: DTU Wind Energy; 2021, p. 62.

[32] Morales-Ruvalcaba C, Rodríguez-Hernández O, Martínez-Alvarado O, Drew D, Ramos E. Estimating wind speed and capacity factors in Mexico using reanalysis data. Energy Sustain Dev 2020;58:158–66. http://dx.doi.org/10.1016/j.esd.2020.08.006.

[33] Turrent C, Zaitsev O. Seasonal cycle of the near-surface diurnal wind field over the Bay of La Paz, Mexico. Bound-Layer Meteorol 2014;151(2):353–71. http://dx.doi.org/10.1007/s10546-014-9908-4.

[34] Morales-Acuña E, Torres CR, Linero-Cueto JR. Surface wind characteristics over Baja California Peninsula during summer. Reg Stud Mar Sci 2019;29:100654. http://dx.doi.org/10.1016/j.rsma.2019.100654.

[35] Barrera Bassols N, Palma Ruiz A. Geografía. 1st ed.. Xalapa, México: Secretaría de Educación de Veracruz; 2008.

[36] Pereyra-Castro K, Caetano E, Martínez-Alvarado O, Quintanilla-Montoya AL. Wind and wind power ramp variability over northern Mexico. Atmosphere 2020;11(12):1281. http://dx.doi.org/10.3390/atmos11121281.

[37] Dirección de Capacitación. Características edafológicas, fisiográficas, climáticas e hidrográficas de México.

[38] Programa Forestal Colegio de Postgraduados. Diagnóstico hidrológico-forestal de la región IX-golfo norte. Tech. rep., CONAFOR; 2003.

[39] INECOL, Rzedowski J. Fascículo complementario XXXIV: Catálogo preliminar de especies de plantas vasculares de distribución restringida al eje volcánico transversal. Flora Bajío Reg Adyacentes 2020. http://dx.doi.org/10.21829/fb.305.2020.XXXIV.

[40] Anuario estadístico y geográfico de Oaxaca 2017. Tech. rep., México: Instituto Nacional de Estadística y Geografía; 2017.

[41] Thomas SR, Martínez-Alvarado O, Drew D, Bloomfield H. Drivers of extreme wind events in Mexico for windpower applications. Int J Climatol 2020;joc.6848. http://dx.doi.org/10.1002/joc.6848.

[42] Pérez-Sarabia J, Duno De Stefano R, Fernández-Concha GC, Ramírez Morillo I, Méndez-Jiménez N, Zamora-Crescencio P, Gutiérrez-Baez C, Cetzal-Ix W. El conocimiento florístico de la Península de Yucatán, MéxicoThe floristic knowledge of the Yucatan Peninsula, Mexico. Polibotánica 2017;(44). http://dx.doi.org/10.18387/polibotanica.44.3.

[43] Allende-Arandía ME, Zavala-Hidalgo J, Romero-Centeno R, Franklin GL, Taylor-Espinosa N, Osorio-Tai ME. Large diurnal wind variability over the western and northern Campeche Bank caused by the low latitude of the Yucatan Peninsula and its interaction with Easterlies. Atmos Res 2022;265:105888. http://dx.doi.org/10.1016/j.atmosres.2021.105888.

[44] Castaño González A. Análisis del recurso eólico para la generación eléctrica en distintas regiones de México (Ph.D. thesis), Temixco, México: Universidad Nacional Autónoma de México; 2023.

[45] Skamarock WC, Klemp JB, Dudhia J, Gill DO, Liu Z, Berner J, Wang W, Powers JG, Duda MG, Barker DM, Huang X-Y. A description of the advanced research WRF model version 4. Tech. rep., Boulder: National Center for Atmospheric Research; 2019, p. 162.

[46] Hersbach H, Bell B, Berrisford P, Biavati G, Horányi A, Muñoz Sabater J, Nicolas J, Peubey C, Radu R, Rozum I, Schepers D, Simmons A, Soci C, Dee D, Thépaut J-N. ERA5 hourly data on pressure levels from 1959 to present. 2018, http://dx.doi.org/10.24381/cds.bd0915c6.

[47] Hersbach H, Bell B, Berrisford P, Biavati G, Horányi A, Muñoz Sabater J, Nicolas J, Peubey C, Radu R, Rozum I, Schepers D, Simmons A, Soci C, Dee D, Thépaut J-N. ERA5 hourly data on single levels from 1959 to present. 2018, http://dx.doi.org/10.24381/cds.adbb2d47.

[48] Manwell JF, McGowan JG, Rogers AL. Wind energy explained: theory, design and application. John Wiley & Sons Ltd; 2009.

[49] Simard R, L'Ecuyer P. Computing the two-sided Kolmogorov–Smirnov distribution. J Stat Softw 2011;39(11). http://dx.doi.org/10.18637/jss.v039.i11.

[50] Jaramillo O, Borja M. Wind speed analysis in La Ventosa, Mexico: A bimodal probability distribution case. Renew Energy 2004;29(10):1613–30. http://dx.doi.org/10.1016/j.renene.2004.02.001.

[51] Ács F, Gyöngyösi AZ, Breuer H, Horváth Á, Mona T, Rajkai K. Sensitivity of WRF-simulated planetary boundary layer height to land cover and soil changes. Meteorol Z 2014;23(3):279–93. http://dx.doi.org/10.1127/0941-2948/2014/0544.

[52] López-Espinoza ED, Zavala-Hidalgo J, Mahmood R, Gómez-Ramos O. Assessing the impact of land use and land cover data representation on weather forecast quality: A case study in central Mexico. Atmosphere 2020;11(11):1242. http://dx.doi.org/10.3390/atmos11111242.

[53] Diaz-Esteban Y, López-Villalobos CA, Ochoa Moya CA, Romero-Centeno R, Quintanar IA. Using a hybrid approach for wind power forecasting in northwestern Mexico. Atmósfera 2023;38:263–88. http://dx.doi.org/10.20937/ATM.53258.